Binder-Free N-Functionalized Carbon Electrodes for Oxygen Evolution Reaction

Feihong Song[+],[a] Jan W. Straten[+],[a, b] Yang-Ming Lin,[a, c] Yuxiao Ding,[a, d] Robert Schlögl,[a, e] Saskia Heumann,*[a] and Anna K. Mechler*[a, f]

The oxygen evolution reaction (OER) is one of the bottlenecks of electrochemical water splitting. Metal-free carbons from biomass are highly abundant and can be easily synthesized. Their low price, high conductivity and functionalization makes them promising materials. Herein, we report about free-standing carbon electrodes as electrocatalysts for the OER. In contrast to powder-based catalysts, free-standing electrodes not only avoid additives, but also facilitate post analysis and better reflect industrial conditions. Here, the performance of pure carbon electrodes is compared to those of N-functionalized ones. Utilizing several analytical techniques, the difference in performance can be rationalized by physical properties. Especially, the analysis of the gaseous products is shown to be of crucial importance. It reveals that N-doped carbons generate more oxygen and are more robust against carbon corrosion. This illustrates the importance of measuring selectivity especially for carbon electrocatalysts, as higher currents do not necessarily result in higher catalytic activity.

Introduction

To alleviate the dominance of fossil fuel-based energy resources (e.g. coal, natural gas and oil) and their undesirable side effects such as energy resource depletion and global warming, an increased share of alternative energy sources becomes indispensable. Due to the low energy density of batteries, it is not possible to store sufficient energy to buffer the growing energy demand, at least not as a stand-alone solution.[1] In order to fill this gap, research on multiple energy carriers in gas phase (e.g. H_2 and CH_4), liquid phase (e.g. CH_3OH, redox flow battery) and solid phase (supercapacitor, battery) should coexist at the same time, partially for different applications.[2–6] In this way, the existing infrastructure can be fully utilized towards its full potential. All these studies lead to the same goal: to find alternative energy carriers for future renewable energy conversion processes.

Here, we emphasize on hydrogen as an energy carrier in particular and a process that was found more than 200 years ago, i.e. water electrolysis. Oxygen evolution reaction (OER), the complementary half reaction in electrochemical water electrolysis suffers from sluggish kinetics, and is thus considered as the bottleneck of the whole process. Researchers are eager to find suitable catalysts for water electrolysis. However, many of these catalysts have their distinct drawbacks. For example, iridium and ruthenium-based catalysts, though having superior activity, are limited by high cost and scarcity.[7] In alkaline medium, transition-metal oxide catalysts, for example Ni–Fe, Ni–Fe–Co and Ni–Co catalysts show promising activities. However, the materials themselves are often highly toxic, partially mined under critical conditions and prone to degradation during long-time operation due to metal leaching and increasing electrical resistance.[8–10] Carbon-based materials are frequently used as supports for those metal catalysts, due to their high surface area, high conductivity and high abundance, but themselves can also be proper candidates for OER catalysis.[11–14] Carbon electrodes can produce hydrogen under two conditions, either during the electrocatalytic water splitting process and via carbon corrosion.[15] In the later case, it is used as sacrificial electrode. The technical feasibility has already been demonstrated and carbon materials also offer a wide range of possibilities to further tune the properties for an optimized hydrogen evolution.[15]

In most cases, carbon-based catalysts are prepared as fine powders, which are then dispersed in a slurry and deposited on a supporting electrode (often glassy carbon or gold) for

[a] Dr. F. Song,[+] Dr. J. W. Straten,[+] Dr. Y.-M. Lin, Dr. Y. Ding, Prof. Dr. R. Schlögl, Dr. S. Heumann, Prof. Dr. A. K. Mechler
Max Planck Institute for Chemical Energy Conversion
Stiftstrasse 34–36, 45470 Mülheim an der Ruhr, Germany
E-mail: saskia.heumann@cec.mpg.de
anna.mechler@avt.rwth-aachen.de
[b] Dr. J. W. Straten[+]
current address: Universität Hohenheim,
Institut für Agrartechnik (440f)
Garbenstr. 9, 70599 Stuttgart, Germany
[c] Dr. Y.-M. Lin
current address: Fujian Institute of Research on the Structure of Matter,
Chinese Academy of Sciences
Fuzhou, Fujian 350002, P. R.China
[d] Dr. Y. Ding
current adress: Lanzhou Institute of Chemical Physics
Tianshui Middle Road 18, 730000 Lanzhou, P. R. China
[e] Prof. Dr. R. Schlögl
Fritz-Haber-Institute of the Max Planck Society
Faradayweg 4–6, 14195 Berlin, Germany
[f] Prof. Dr. A. K. Mechler
current address: RWTH Aachen University,
Electrochemical Reaction Engineering
Forckenbeckstraße 51, 52074 Aachen, Germany
[+] These authors contributed equally.

Supporting information for this article is available on the WWW under https://doi.org/10.1002/celc.202201075

electrochemical measurements.[16] For a good integrity of the carbon catalysts on those supports, the use of ionomers/binders is often necessary and the catalyst layer formed on the conductive substrate is usually inhomogeneous due to the "coffee ring" effect.[17] Also the classical testing via rotating disc electrode tends to be less reproducible for thin-film electrodes and is affected by several external parameters.[18] The additional ionomer and interplay with the support electrode under the electrocatalysis process can influence the intrinsic properties of the catalyst itself, for example by catalyst-support interaction,[19] thereby adding further complex parameters for finding the structure-function relationship. The drop-casting method also builds an application gap towards industry, where typically bulk, porous electrodes are used, resulting in the necessity of additional scaling processes that have to be investigated later on. With our approach, we are able to produce binder-free, free-standing carbon electrodes, thus making the electrochemical tests more meaningful and realistic. In addition to that, our approach also paves the way for post-electrochemical analysis, which is very difficult for the small amounts of catalysts supported on a working electrode for e.g. rotating disk electrode measurements.

N-functionalized carbon is considered as a promising OER or ORR catalyst by changing the local electron density near the carbon atoms.[20,21] The addition of heteroatoms into the carbon network tailors their band structure, while at the same time maintaining a good conductivity.[22–24] Although a boosting effect of N-doping was found,[25] where the researchers suggested that the active sites for ORR/OER are close to the carbon adjacent to the pyridinic N, no clear evidence for one specific active species is found yet. Moreover, the corrosion or degradation of carbon-based OER catalysts were not well studied and are rarely considered in literature.[26–29] Also with respect to stability, the nature of the functional groups were proposed to influence the stability, for instance pyrrolic and pyridinic N sites were calculated to be more stable than graphitic N.[29] Here, we demonstrate that indeed nitrogen species in the carbonaceous electrode not only provide active functional groups for the OER, but also slow down the carbon corrosion process, leading to an improved selectivity towards O_2 instead of CO or CO_2.[30] We believe this to be a synergistic effect of improved conductivity and more active-sites that prefer the OER over corrosion.

Results and Discussion

The free-standing carbon electrodes utilized in this work were prepared by hydrothermal synthesis, denoted as HTC or NHTC if prepared with an addition N-source, respectively. Four different disc electrodes were synthesized by variation of the hydrothermal temperature and the amount of urotropine (N precursor). An overview of the preparation conditions as well as the resulting elemental composition measured by elemental analysis are listed in Table 1 and the supporting information. HTC-180 and NHTC-high-250 samples could not be prepared, because the carbon pellets were deformed after pyrolysis. All electrodes have diameters around 10 mm (±0.2 mm) and thicknesses of about 1 mm (±0.1 mm).

As can be seen in the atomic ratio of elements, the amount of N was successfully altered by adjusting the amount of urotropine precursor from 12 g (low) to 37.2 g (high). NHTC electrodes have up to five times higher N content compared to HTC-250 according to the elemental analysis. The remaining of the N in HTC sample may originate from impurities in the precursors. Besides, by comparing NHTC-low-180 and NHTC-low-250, increasing the hydrothermal synthesis temperature from 180 to 250 °C has negligible influence on the atomic ratio.

The conductivity of the HTC/NHTC electrodes were measured by the van der Pauw method, which is especially suitable for thin (thickness/diameter $\leq$0.1) disc electrodes and helps to overcome the problem of contact resistance by using a four-points probe. Figure S1 displays the conductivity of HTC and NHTC disc electrodes. Remarkably, HTC-250 annealed at 1000 °C already shows one order of magnitude higher conductivity compared to other reported biomass-derived hydrothermal carbon materials.[31] In addition, the introduction of N leads to a significant conductivity gain. The overall more agglomerated structure (with less grain boundaries) of NHTC may contribute to the improved conductivity. While the conductivity increases with increasing N-content (i.e. from NHTC-low-180 to NHTC-high-180) by a factor 1.5, increasing the hydrothermal temperature from 180 °C to 250 °C is rather detrimental.

SEM images, shown in Figure 1, reveal that the HTC materials consist of carbon spherical particles forming an interconnected network of the spheres. For pure HTC (HTC-250), the average particle size is about 0.6–0.8 μm and relatively homogeneous. The introduction of N increases the carbon sphere size by almost a factor of 10 (4–8 μm) and the size distribution becomes less homogeneous.

The surface functional groups of HTC-250 and NHTC-low-250 disc electrodes were analyzed by XPS. For HTC-250 no N 1s in the spectrum could be measured, while NHTC-low-250 shows

Table 1. Sample nomenclature depending on the synthesis conditions, and the elemental composition from elemental analysis given in at.%. As only C, H, and N can directly be measured, the remaining mass is assigned to Oxygen.

Sample name	Description	C	H	N	Rest = O
HTC-250	no N, hydrothermal T: 250 °C	97.7	0.6	0.7	1.0
NHTC-low-180	low N content, hydrothermal T: 180 °C	95.3	0.7	3.5	0.5
NHTC-low-250	low N content, hydrothermal T: 250 °C	95.3	0.5	3.5	0.7
NHTC-high-180	high N content, hydrothermal T: 180 °C	93.3	0.6	5.1	1.0

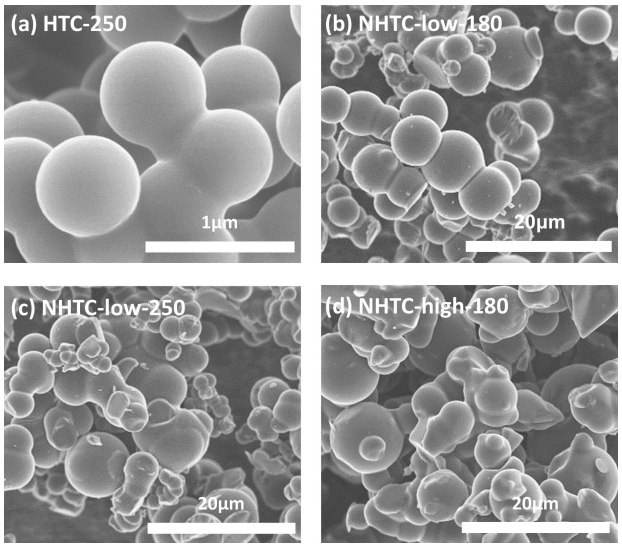

Figure 1. Scanning electron microscopy (SEM) images of the hydrothermal carbon after pressing and annealing at 1000 °C for 5 h for (a) HTC-250; (b) NHTC-low-180; (c) NHTC-low-250; (d) NHTC-high-180.

both O 1s and N 1s peak. The small amount of N in HTC-250 found by elemental analysis may be inhomogeneously dispersed or not present on the surface and thus not detected by XPS. The O 1s spectra are depicted in Figure 2a and 2b, where they are divided into four and five regions for HTC-250 and NHTC-low-250, respectively. The O 1s spectrum of HTC-250 is deconvoluted into the following regions: O1 (531.0 ± 0.3 eV) corresponding to carbonyl (C=O) groups, O2 (532.3 ± 0.2 eV) assigned to ether-like (C–O–C) single bond, O3 (533.5 ± 0.3 eV) to phenol (C–OH) groups and O4 (534–535 eV) to surface OH (from adsorbed water).[32,33] NHTC-low-250 has one extra region (530.3 eV) assigned to pyridonic O (NC=O) due to the presence of N in the carbon structure. Through peak fitting of N 1s

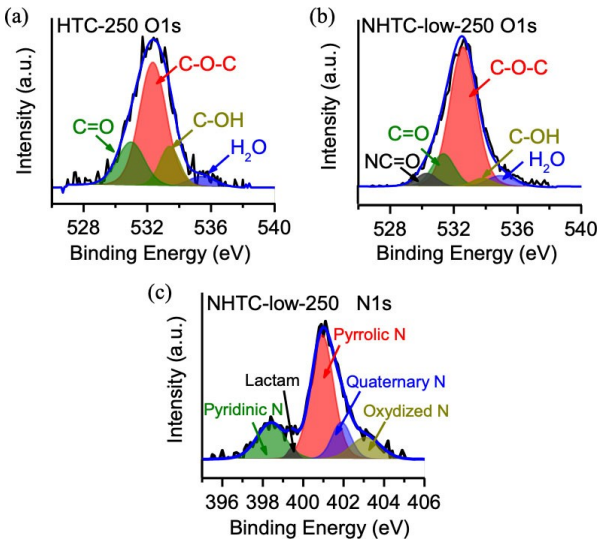

Figure 2. XPS spectra of the O 1s emission of (a) HTC-250 and (b) NHTC-low-250, (c) N 1s emission of NHTC-low-250.

spectra of NHTC-low-250 (Figure 2c), the possible surface N species can be revealed. The N 1s spectra are deconvoluted into five peaks, i.e. N1 (Pyridinic N), N2 (Lactam or Amine groups), N3 (Pyrrolic N), N4 (Quaternary N) and N5 (Oxidized N), at 398.4 eV, 399.5 eV, 400.9 eV, 401.9 eV and 403.1 eV, respectively.[34,35] The most abundant N functional group is pyrrolic N, following by pyridinic N and quaternary N. Also, Amine or Lactam groups as well as oxidized N can be found. The C1s spectra of both electrodes are reported in Figure S2, where a dominant peak around 284.3 eV corresponding to sp^2 carbons for both HTC and NHTC electrodes was found.

To apply the (N)HTC disc electrodes for electrochemistry, a proper wetting of the surface is a prerequisite. The surface wetting properties of the carbon electrodes were measured using a drop shape analyzer. Figure S3 presents the dynamic contact angle scenario, where a water droplet was absorbed into the porous structure in rather short time frame. Only the HTC-250 sample has a clear tendency of absorbing water, indicating a hydrophilic surface. In contrast, for all NHTC electrodes the contact angles are much higher, indicating a hydrophobic surface of the electrodes. In Figure S3c it can be seen that even after 10 min a droplet was not fully absorbed into an NHTC-low-250 electrode. In order to improve the electrode wetting already before the experiment, the NHTC electrodes were hence soaked in 0.1 M KOH overnight before electrochemical tests. Furthermore, the dynamic contact angle measurement was repeated after the first conditioning step, where the initial contact angle was significantly reduced and the droplet was quickly absorbed into the pellet (Figure S3c). Hence, it can be assumed that latest during this first conditioning step a full wetting of the electrodes was achieved.

The electrochemical performance of all electrodes were measured in a stationary electrochemical cell made by PEEK in a three-electrode configuration (see Experimentals). A defined protocol (i.e. four loops measurements), which measures the capacity, activity and stability in four consecutive loops was used (Figure S4). In short, each loop includes, in sequence, capacitance cyclic voltammetry (CV), activity CV, stationary polarization and chronopotentiometry tests. The four loops measurement protocol allows the investigation of characteristics (capacitance, activity, stability, etc.) change over time by comparing the performance in each loop.

Figure 3 shows the full set of loop experiment results of NHTC-low-250 as an example. To exclude the influence from dissolved oxygen, a controlled four loops measurement was carried out with the same sample in Ar purged electrolyte. The result (Figure S5) shows no difference compared to Figure 3b. Figure 3a compares the conditioning cycles, recorded at low potential between 0.2 and 1.2 V, which are featureless and consist solely of capacitive current. It is worth to mention that the capacitive current may also include electrochemical redox reactions of surface (oxygen)functional groups. The double layer capacitance of the NHTC electrode dramatically increased after loop 1, possibly indicating an increase in electrochemical active surface area, or the formation of functional groups. After further increment of capacitance in loop 2, the capacitance starts to decrease in loop 3 as a result of mechanical detachment of

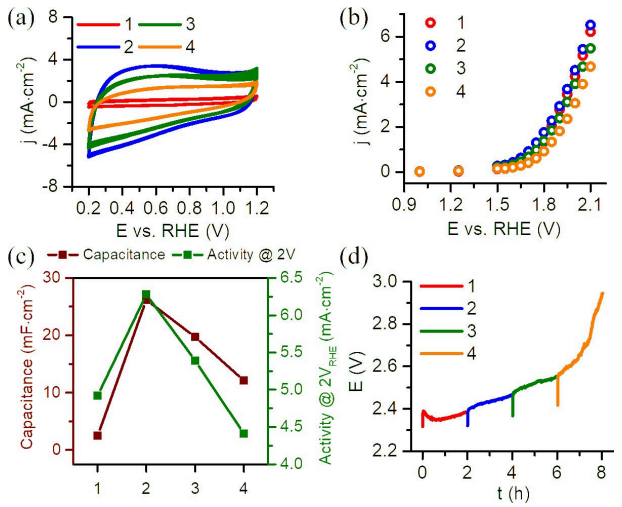

Figure 3. Electrochemical measurements (i.e. four loops measurements) of NHTC-low-250 in 0.1 M KOH. The numbering 1 to 4 represents the consecutive measurement loop. (a) Capacitance cyclic voltammetry (CV) curves at scan rate of 100 mV s^{-1} with iR correction. (b) Stationary polarization technique, where a series of constant potentials were applied for 2 mins. Each current data is collected by averaging the last 30 s of the current signal. (c) Comparison of capacitance and activity in different loops, x-axis indicates the loop number. (d) Chronopotentiometry (CP) at constant current density (10 mA/cm^2) for 2 h in each loop, for a total of 8 h.

small carbon solid particles. In Figure 3b, at relatively high potential (> 1.5 V), the current follows the same trend as the progress of the capacitance, where the current firstly increases and then decreases after loop 3. The trend of the capacity and activity are summarized in Figure 3c. The increase of capacitance and activity current might be explained by the removal of disordered carbon species and the formation of more surface (oxygen)functional groups. Whereas the decrease after the 2nd cycle may be mainly attributed to the carbon corrosion reaction, which can lead to a saturation of functional groups on the carbon surface as well as loss of electrical conductivity. Finally, for the Chronopotentiometry (CP) test shown in Figure 3d, under even higher potentials (> 2 V at 10 mA/cm^2), the carbon oxidation plays a critical role as indicated by the increase of potential over time.

During the 2 hour CP test in loop 1, the amorphous carbon within the electrode was likely oxidized and removed from the backbone structure, leaving more surface exposed to the electrolyte, and thus leads to the massive increment of capacitance in loop 2 compared to loop 1, as displayed in Figure 3a. This scenario can also be explained by the formation of new surface functional groups, especially acidic groups (e.g. -COOH), which increase the capacitance by pseudo-capacitive effects.[36] The continuous increase of potential in the CP test (Figure 3d) within each consecutive measurement loop can also be interpreted by the following: as the pores gradually develop because of carbon oxidation, the pH value inside the pores of the NHTC electrode decrease due to the OER and carbon oxidation reactions (both consume OH^-). Consequently, the decrease of local pH value inside the pores, according to Nernst law, leads to a positive potential shift for the OER as well as a decrease of ionic conductivity in the solution phase.

Optically, the electrolyte slowly changes from colorless to brownish color because of the formation of soluble byproducts, which normally exist in low concentration.[37] ESI-MS results (Figure S6) show that only minor soluble molecules (m/z > 90) were found in the electrolyte after the whole test. UV-Vis measurement of the used electrolyte (Figure S7) after the full four loops reveals the presence of soluble aromatic molecules (e.g. humic acid compound)[38] by the broad adsorption band. In fact, during loop 4 some parts of the electrode that were immersed into the electrolyte starts to peel off during the CP measurement and small particles can be found at the bottom of the container, which leads to the drastic increase of the potential (> 2.5 V). At this stage, also the conductivity of the electrode might already be significantly decreased as the interconnected microscopic carbon structures were destroyed. A study by Yi et al.,[26] showed that the electrochemical oxidation of glassy carbon in alkaline media first starts on the edges to form carboxylic acid groups on the surface until the π-π interaction between the carbon flakes and glassy carbon becomes weaker and dissolve in the electrolyte. This theory could also be applied to our carbon electrodes to explain the corrosion mechanism towards dissolution of larger carbon compounds.

$$C + 2H_2O \rightarrow CO_2 + 4H^+ + 4e^-, \quad E_1^0 = 0.207\ \text{V vs. SHE} \tag{1}$$

$$C + H_2O \rightarrow CO + 2H^+ + 2e^-, \quad E_2^0 = 0.518\ \text{V vs. SHE} \tag{2}$$

According to Eq. (1) and Eq. (2), one would expect the formation of CO_2 should be the main product as its formal potential is lower compared to that of CO formation and thus thermodynamically favorable. The main corrosion product CO_2 remains in the solution phase by reacting with KOH to form K_2CO_3, proved by electron-spray ionization mass spectrometry (Figure S6), where the ionization product HCO_3^{1-} (m/z = 61) and CH_3OCOO^- (m/z = 75, from esterification reaction with measurement solvent (CH_3OH) were found as main peaks. Both HCO^- and CH_3OCOO^- originate from the CO_3^{2-} groups in the used electrolyte. The four loops measurement results of other electrodes can be found in Figure S8-S10. There are huge performance disparities between HTC-250 and all the NHTC electrodes. HTC-250 has about 10 times higher capacitance as well as higher activity current compared to NHTC electrodes. Furthermore, after loop 1, the HTC-250 electrode performance begins to deviate dramatically from its initial performance characterized by (i) a huge increase of capacitive current at low potential range (1–1.2 V) in both capacitance CV and activity CV with a tilted CV shape indicating of resistivity increment, (ii) a current plateau at high potential region (> 1.8 V) in the stationary polarization test and (iii) a sharp increase of potential in the CP test already in the second loop. All these changes suggest fast corrosion and deactivation of the HTC-250 electrode. NHTC-low-180 and NHTC-high-180 electrodes per-

form similar to that of NHTC-low-250 as discussed before, except that their chronopotentiometry test has no sharp increase in loop 4 due to likely better mechanical stability.

The electrochemical performance, including double layer capacitance, activity and stability of different carbon electrodes, is compared in Figure 4. Measurements of each sample were repeated at least once to ensure reproducibility. The parameters used in the figure are defined as follows and defined in more detail in the Experimental section. The capacitance is obtained from the last cycle in the capacitance CV. The "Current density@2 V" is the determined current density from the activity CV measurement at 2 V vs. RHE from the 2nd loop, as in loop 1 all the electrodes were undertaking activation process and the electrode performance was changing continuously. The stability is calculated as the relative potential drop during the CP from the beginning of the first loop (E_0) to the end of the last loop (E_{end}). Those characteristic performance indicators clearly show differences between the NHTC and HTC materials. The HTC electrode presents much higher capacitance as that of NHTC, which correlates well with the smaller carbon particle size, as smaller particle size generally has higher surface area. Also, the maximum current density of the HTC disc electrode is triple that of all NHTC electrodes. Note that this does not necessarily correlates with a higher activity towards OER, as we will show later that HTC-250 produces rather CO/CO_2 than O_2. Moreover, the current densities change during the measurement time, especially if you look at the stationary polarization tests (Figure S8–S10). In agreement with this, most NHTC electrodes show better stability than HTC-250. Especially, NHTC-high-180 (b) and NHTC-low-180 (c) retain more than 90% of their initial potential at 10 mA/cm^2. Interestingly NHTC-low-250 shows a relatively low stability similar to that of HTC. However, before the last loop, the potential only increased by 6%, indicating a mechanical failure rather than a continuous degradation process. The increase of N content, from NHTC-low-180 to NHTC-high-180, has little influence on the electrochemical performance, as in the spider graph both have similar activity, capacity as well as stability.

To better understand the surface state of the electrodes before and after electrochemistry, the work function of the electrodes were measured by Kelvin Probe (KPTechnology, England) at room temperature. All samples were stored in a desiccator and heated to 100 °C overnight to remove surface adsorbed water before measurement. To ensure the data accuracy and calculate the standard deviation, all the measurement were repeated three time on three different samples of each type. The work function is the minimum energy (in eV) required to emit an electron to a point in vacuum outside the

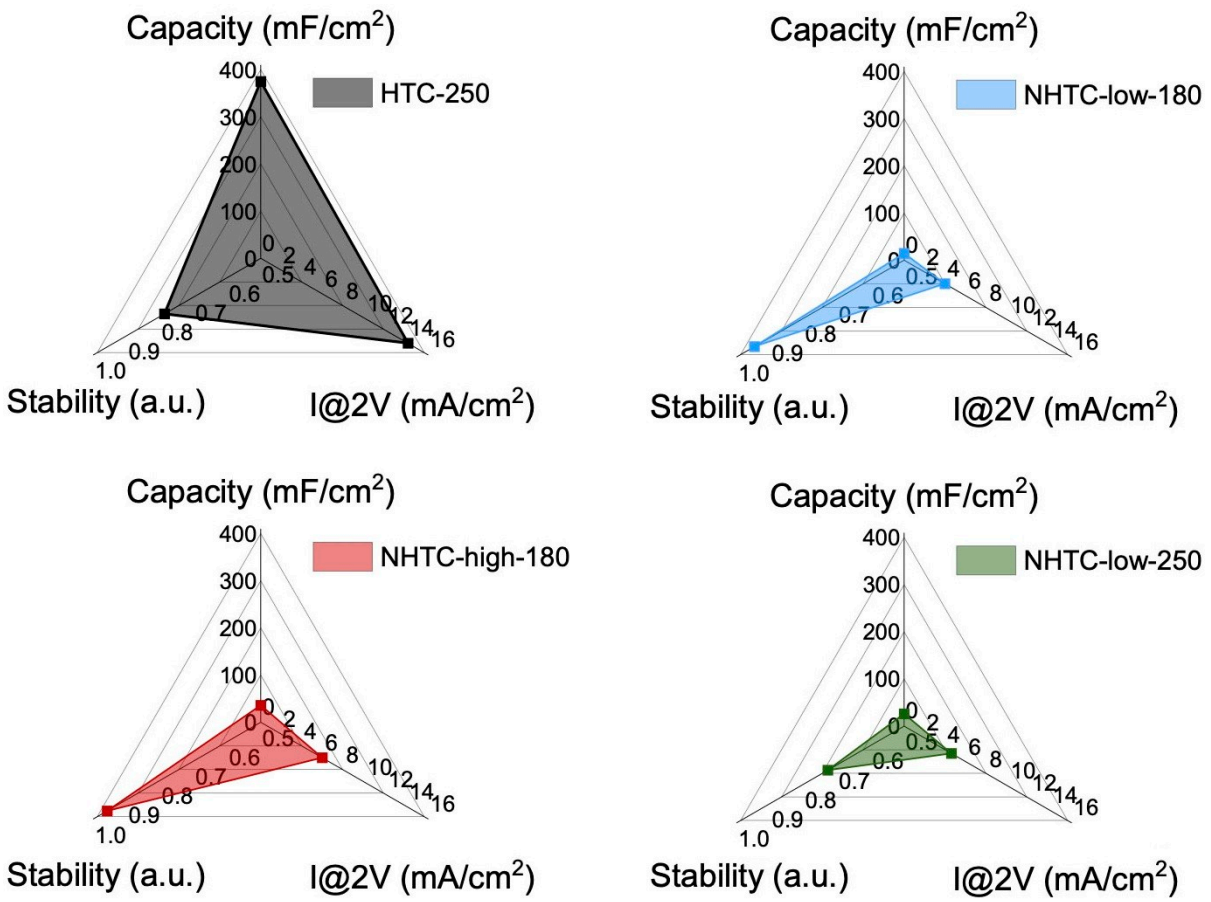

Figure 4. Comparison of electrochemical performance, including capacity (mF/cm^2), stability (uniform unit) and activity (mA/cm^2) between HTC and NHTC electrodes: (a) HTC-250, (b) NHTC-low-180, (c) NHTC-low-250 and (d) NHTC-high-180.

solid surface and it corresponds positively with the ionization energy of the surface.[39] As a surface sensitive property, the work function can be used to monitor the surface change during the electrochemical processes. As the transfer of an electron from or to the electrode is a prerequisite for a reaction, one might predict that those electrodes with lower work function should have higher activity/current under electrochemical conditions, even though the reaction could also be carbon corrosion instead of OER. In Figure 5a, the WF of the pristine HTC-250 electrode is about 50–80 meV lower than pristine NHTC electrodes. As reference, the WF of HOPG (highly oriented pyrolytic graphite) is around 4.5 eV.[40] However, after the conditioning step in loop 1, the work function of all 4 electrodes decreased dramatically by more than 200 meV. This change might be associated to the formation of surface functional groups during the conditioning cycle.[41] After the four loops measurement protocol, the work function of all carbon electrodes has an increase of roughly 50 meV, meaning the surface is harder to be ionized (oxidized). At this stage, the surface of the electrode might become "passivated", and therefore requires more energy to emit electrons.

After the four loops measurement, the electrode was washed with DI water and tested with XPS. The XPS survey spectra of NHTC-low-250 after four loops measurement (~8 h of high potential operation) can be found in Figure S11. The result shows that the oxygen content increases drastically after the electrochemical measurement. Metal impurities (K, Na, Ca) in the KOH can also be found, although the electrode was intensely washed with DI water before XPS measurements, indicating that the impurities are bonded chemically to the surface oxygen groups. The C1s spectra (Figure S12) can be deconvoluted into different species including oxygen functional groups (C–O, C=O, COO_2) and metal carbonate, which correlates to the carbon surface oxidation and the formation of CO_2, respectively. At this stage, the carbon electrode surface might be extensively covered by oxygen species. The O 1s spectra was not fitted due to the peak overlapping between metal carbonate and carbon oxygen functional groups. In addition, the N 1s spectra (Figure S13) become less intense compared to the pristine sample. Possibly, N-functionalities were degraded in the course of the experiment.

Apart from the OER, thermodynamic oxidation of carbon, although exhibiting slow kinetics, inevitably occurs according to Eq. (1) and (2), which are considered as side reactions. The detection of the product gases in combination with electrochemical test provides unique insights into the occuring reaction of different samples, i.e. between HTC and NHTC electrodes. To investigate the influence of N-doping under similar preparation conditions on the performance of the electrode, we focus in the following on the comparison of HTC-250 and NHTC-low-250 electrodes.

Gas-phase detection is very important to monitor the actual activity and quantitatively compare the gas products from different carbon disc electrodes. A special gas collection cell was designed, which was sealed from atmosphere during the measurement (cell design see Figure S14) and used to collect the gaseous products. Before the experiment, the cell was purged with Ar over night to achieve full saturation. Then a small dose of gas products (50 µL) was collected with a needle-syringe (with lock function) and injected into a mass spectrometer (MS) under a continuous flow of Ar (carrier gas). The obtained spectra were used as a background signal. Due to the low current densities even at elevated potentials (< 10 mA/cm^2@1.8 V), the produced gas was accumulated over 18 h. Beside the signal for O_2 as product, additionally the signals $[C]^+$ at m/z = 12 (fragmentation of both CO_2 and CO) were monitored (Figure 6). Samples were collected and introduced into the MS and corrected by subtraction of the background signal. The corrected peaks of $[O_2]^+$ and $[C]^+$ can be found in Figure S15. Although the gas collection was performed under the same applied potential for both electrodes, the currents were not the same (Figure S16) and therefore the total amount of gas produced should be different. Additionally, CO_2 can be

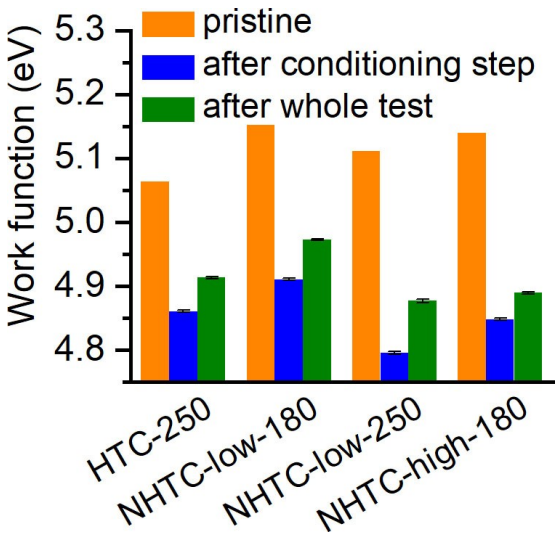

Figure 5. Work Function (WF) of the HTC-250 and NHTC electrodes before (pristine) and after the conditioning step in loop 1 and after the entire four loops electrochemistry test.

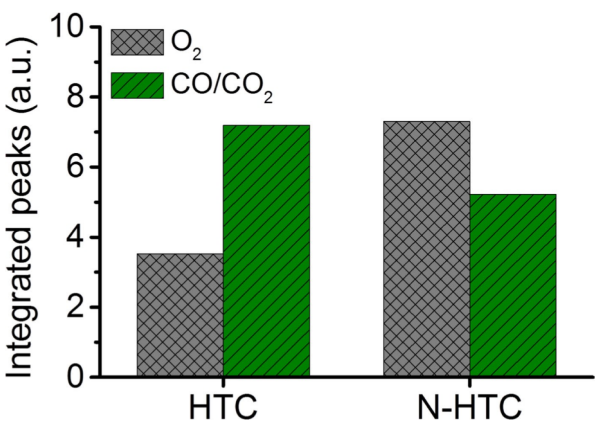

Figure 6. Mass spectrometry integrated peak areas of $[O2]^+$ (m/z = 32) and $[C]^+$ (m/z = 12) corresponding to ion fragments of CO/CO_2 for HTC (i.e. HTC-250) as well as NHTC (i.e. NHTC-low-250) after 18 h of gas product accumulation at 1.8 V.

expected to dissolve at least partially in the alkaline electrolyte. A direct comparison of the gas quantities is therefore not possible, nevertheless the ratios can be compared. In literature it is discussed that nitrogen in carbon based electrodes has a positive effect in favor the electrocatalytic OER reaction and therefore producing more O_2 than CO/CO_2.[20,22,25,42] This observation is supported by the gas analysis data. The peak of CO/CO_2 fragmentation at m/z = 12 for the NHTC electrode has lower integrated peak area than HTC, indicating the NHTC is more corrosion-stable compared to HTC. The formation of CO/CO_2 is probably due to the elimination of aromatic functional groups (phenol, quinones, aromatic acids, etc. bonded to aromatic carbon) by carbon oxidation reaction, which also leads to the removal of functionalized sp^2 carbon on the electrode surface and possibly also the loss of conductivity.[43] Additionally, relatively more O_2 was produced with the nitrogen modified electrode.

In order to follow the dynamic behavior of both HTC and NHTC electrodes over a much longer time-frame, a simple Hofmann apparatus (Figure S17) was used to record the gas product volume over time. In brief, the Hofmann apparatus consists of two electrodes with Pt as cathode and carbon disc electrodes of interest as anode. The gases were collected separately from each side, while it is assumed that the gas on the anode site mainly contains O_2 and CO (CO_2 exists in the liquid phase as K_2CO_3), while at the cathode H_2 is collected. Figure 7a and 7b show the normalized product gas volume under constant applied potential of 2.4 (±0.1) V for NHTC within 360 h and HTC within 220 h, after which the electrodes were physically significantly corroded. Regarding the cathode sides of the two electrodes ((N)HTC), they behave similarly, seeing that the total amount of H_2 produced was similar and both increased over time, while the slope of the curves (or the H_2 production rate) from both electrodes gradually decreased as the current (initially about 10 mA) also dropped slightly. From the H_2 curve, a theoretical O_2 production curve (blue curve in Figure 7a) can be predicted, assuming an ideal stoichiometry of $H_2:O_2 = 2:1$. Regarding the anode sides, the two electrodes behave differently. For NHTC within the first ca. 50 h, the anode gas product volume is close to the theoretical oxygen volume, indicating the production of O_2 accompanied by little or no energy loss to the carbon oxidation reactions. However, as the test continues, no further increase of gas volume was observed, i.e. the oxygen evolution was no longer being catalyzed. This was observed in our previous studies investigating the feasibility of carbon-based electrodes as well.[15] Instead, the current might drive carbon oxidation, producing CO_2, which will then react with KOH to form K_2CO_3. As we observed that N-functionalities were reduced after the four-loops measurement (Figure S13), it is reasonable to assume that they were also degraded during this continuous experiment. This would indicate that N-functionalities are necessary to catalyze the OER, while if they are removed mainly carbon corrosion occurs. For the HTC electrode, almost no gas product was observed on the anode side for the whole duration and the electrode was completely destroyed after 220 h, while NHTC lasted almost double the lifespan (360 h). This phenomenon further proves that the NHTC electrode is more corrosion-resistant and more active for OER compared to the HTC electrode.

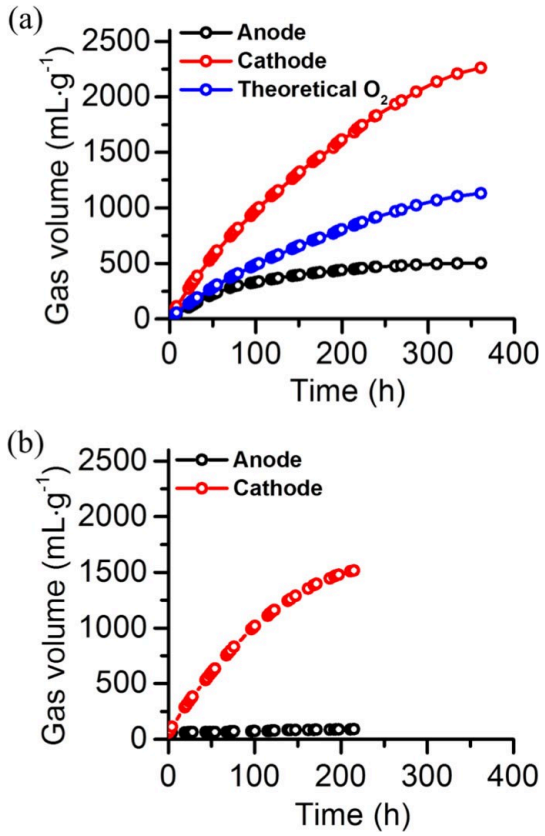

Figure 7. Volumetric gas detection by Hofmann apparatus for (a) NHTC-low-250 and (b) HTC-250, respectively. The theoretical oxygen volume in (a) is calculated as half of the cathode gas volume ($H_2:O_2$ stoichiometry 2:1). The detected volume was normalized to the weight of the respective catalyst pellet.

Conclusion

In summary, instead of using the conventional drop coating method, our facile and industrial applicable fabrication method of free-standing carbon electrodes casts a new light on the preparation of carbon-based electrocatalysts. The simple synthesis method not only gets rid of the binder materials, but also facilitates the post electrochemical analysis by optical and physical methods (e.g. XPS and work function). At various applied potential regions, different charge transfer processes were observed including double layer charging and formation of oxygen-functional groups. Different N species found by XPS (i.e. significant amounts of pyrrolic and pyridinic N) in the NHTC carbon electrode seem to improve the selectivity towards OER and also reduces carbon oxidation in alkaline media. This phenomenon was directly monitored by mass spectrometry, where a higher O_2 peak area and at the same time a lower CO/CO_2 peak area was found. Hofmann measurements also indicate that NHTC produces more O_2, which is consistent with the mass

spectrometry results. It was also found that the amount of N-functional groups is decreased during electrochemical operation, as shown by post-electrochemical XPS, and for instance in the Hofmann measurements the OER contribution was reduced after about 50 h of operation. Unfortunately, due to a large mixture of N-functional groups as well as O-functional groups evolving in the course of the reaction, a clear assignment of the activity as well as stability enhancement to specific N-functional groups cannot be deduced from the current results. These mechanistical understanding would be interesting to study in follow-up works. The results underline the importance to recognize that the electrochemical current, measured at one point rather than in a long-term measurements, cannot by default be related to the OER activity, especially for carbon containing electrocatalysts, which can change over time and be oxidized at high applied potential. As we have shown, although HTC initially has superior current densities at high applied potentials, it produced less O_2 and likely more CO/CO_2 than NHTC, indicating poor selectivity towards the desired product. The improvement of overall performance by adding N, i.e. improvement of selectivity towards OER and long-term stability, might be a synergistic effect of enhanced connection between carbon networks, and hence improved conductivity, and more active sites (for OER) in the vicinity of N atoms. Possible reasons for the degradation are the loss of active surface area, a continuous carbon oxidation increasing O- and decreasing N-functional groups, the drop of local pH inside the pores resulting in a higher onset potential for the OER, as well as a decrease of overall conductivity due to mechanical destruction.

Overall, the results indicate that N-doping of carbon is a promising approach to increase the selectivity for OER and suppress carbon corrosion. This also stresses the importance to monitor gaseous products, even for a single expected product gas, in order to consider the selectivity when evaluating new (carbon-based) electrocatalysts.

Experimental Section

Carbon Electrode Synthesis

The detailed synthesis of free-standing carbon electrodes, labeled as hydrothermal carbon (HTC) electrode and nitrogen-functionalized hydrothermal carbon (NHTC), is reported elsewhere.[44] In short, glucose (Sigma–Aldrich, Germany), is mixed with deionized water (DI water), and then transferred to a Teflon-lined autoclave for hydrothermal treatment at 180 °C or 250 °C. Urotropine (Sigma–Aldrich, Germany) was additionally added and mixed with glucose solution to obtain NHTC. All chemicals used in this work are of analytical grade. After the hydrothermal treatment, the hydrochar was pressed (using hydraulic press at 10 bar for 2 mins) and annealed at 1000 °C for 5 h under Ar atmosphere. During this post-treatment, the functional groups lead to an intrinsic sintering and linking of the carbon powders into a stable, porous electrode. A more detailed description of the electrodes synthesis can be found in Table S1.

Physical Characterization

The conductivity measurements of the pellet-shaped carbon electrodes were performed using a four point probe precise resistivity measurement device (HIOKI 3541 resistance HiTester, Japan) according to the van der Pauw method.[45] The carbon disc electrode was pasted with Ag contacts around its perimeter. In total four contact points were applied on the carbon disc electrode and they were separated from each other by 90°. A home made MATLAB program was used to solve the van der Pauw equation.

Scanning electron microscopy (SEM) images were acquired on a FESEM SU8020 (HI-TACHI, Japan) with secondary electron detectors.

In order to confirm the nitrogen species on the carbon surface, X-ray photoelectron spectroscopy (XPS) was recorded using a PHI 5000 VersaProbe spectrometer (Physical Electronics, US) with monochromatic Al K-α incident X-ray. The high resolution spectra were taken at a pass energy of 23 eV with a step size of 0.1 eV in ultra-high vacuum. The as-synthesized carbon disc electrodes were directly used for the XPS measurements. XPS spectra were deconvoluted using mixture function of Lorentzian and Gaussian by subtraction of the Shirley background and applying constraining of 1.4–2 eV to the full-width at half-maximum (FWHM) and defining the peak position within $\pm$0.3 eV.

Work function measurement of HTC/NHTC electrodes (pristine, after electrode conditioning step and after complete electrochemical measurement) were conducted using a Kelvin probe instrument (KPTechnology, England). The Kelvin probe is equipped with a vibrating tip in the close vicinity to the sample surface. A voltage bias of 7 V was applied between the sample and the tip. The absolute work function of the sample is calibrated by using pure Au foil (99.9%, Goodfellow, Germany).

Contact angle measurements were conducted by a drop shape analyzer from KRÜSS (Germany) with a high precision camera to record the dynamic contact angle as well as droplet volume at the same time.

The electrolyte solution after electrochemical test was analyzed by a standard electro-spray ionization mass spectrometry (abbreviated as ESI-MS, Thermo Scientific, US). UV/Vis spectra of the post reaction electrolyte was measured by Cary 8454 UV/Vis spectrometer from Agilent Technologies (US) in 5 mm cuvettes.

Electrochemical Characterization

The electrochemical measurements were carried out using a Biologic VMP3 potentiostat (France) using a standard three electrode configuration in a beaker-shaped cell made from PEEK. Prior to each experiment, the electrochemical cell was cleaned in a beaker with boiled DI water. A graphite rod and Hg/HgO (0.1 M KOH) were used as counter electrode (CE) and reference electrode (RE), respectively. The RE was calibrated with respect to a reversible hydrogen electrode (RHE). The as-synthesized carbon electrodes were immersed into the electrolyte to get properly soaked over night, and directly used as working electrode (WE) without further treatment. The WE holder is made by PTFE and equipped with a Pt sheet to achieve electrical contact with the HTC/NHTC electrodes. All measurements were corrected for the electrolyte resistance (iR). For proper comparability of the different samples a defined measurement protocol was utilized. The detailed measurement protocol, denoted as "four loops measurements", is illustrated in Figure S4. The capacitance is obtained from the last cycle of the conditioning CV, which is calculated using Eq. (3).

$$Capacity = \int (I \cdot dV)/(v \cdot \Delta V) \quad (3)$$

where I is the response current density, v is the potential scan rate and ΔV is the potential range. The "Current density@2 V" is defined as the current density at 2 V vs. RHE in the activity CV measurement of the second loop. The stability is calculated as the potential drop during the chronopotentiometry (CP) from the beginning of the first loop (E_0) to the end of the last loop (E_{end}) according to Eq. (4).

$$Stability = 1 - (E_{end} - E_0)/E_0 \quad (4)$$

Gaseous Product Analysis

A mass spectrometer (OmniStar GSD 320) from Pfeiffer Vacuum was employed for the product gas analysis. Ar carrier gas was connected and flown continuously through the mass spectrometer capillary inlet, where a small dose of analyze-gas (typically 50 μL) was injected through a septum. The cell used for the gas collection (denoted as "gas collection cell") is depicted in Figure S14, with a total volume of 180 mL. The cell is made by PEEK and designed to be gas tight. The used electrodes were the same as in the classical electrochemical experiment. The reaction product-gas was collected from the gas collection cell using a gas-collecting syringe with replaceable cone tip needle (Trajan, Australia). The cell was purged with Ar overnight prior to the measurement. The collection duration is set to 18 h in order to accumulate enough gas for analysis with constant applied potential at 1.8 V vs. RHE. For a typical measurement, 130 mL of 0.1 M KOH was employed as electrolyte.

As a second approach, a Hofmann apparatus was used for collecting gases during water electrolysis. The setup consists of an anode (carbon electrode of interest) and a cathode (Pt sheet). It was employed for the quantitative evaluation of the water splitting product gas volume over time. The Hofmann apparatus was filled with 0.1 M KOH. A constant voltage of 2.4 V was applied between the two electrodes. A schematic illustration of the Hofmann apparatus can be found in Figure S17.

Acknowledgements

The authors would like to thank Dr. Mark Greiner and Gudrun Klihm from MPI CEC for assisting XPS measurements, Natalia Jakobs and Teresa Stamm from MPI CEC for the help of the hydrothermal synthesis of HTC and NHTC materials. Dr. Huiqing Song from the MPI CEC for helping the construction of MS system and Dr. Heeyong Park from MPI CEC/Forschungszentrum Jülich IEK-9 for the SEM measurements. Furthermore, Dr. Sebastian Tigges from MPI CEC is acknowledged for performing additional contact angle measurements. The authors also would like to thank the Max Planck Society as well as the IMPRS-SurMat for financial support. Open Access funding enabled and organized by Projekt DEAL.

Conflict of Interest

There are no conflicts of interest.

Data Availability Statement

The data that support the findings of this study are available from the corresponding author upon reasonable request.

Keywords: carbon · degradation · nitrogen doping · oxygen evolution reaction · water splitting

[1] M. Asadi, B. Sayahpour, P. Abbasi, A. T. Ngo, K. Karis, J. R. Jokisaari, C. Liu, B. Narayanan, M. Gerard, P. Yasaei, X. Hu, A. Mukherjee, K. C. Lau, R. S. Assary, F. Khalili-Araghi, R. F. Klie, L. A. Curtiss, A. Salehi-Khojin, *Nature* **2018**, *555*, 502.
[2] Z. Jiang, K. Klyukin, V. Alexandrov, *Phys. Chem. Chem. Phys.* **2017**, *19*, 14897.
[3] J. Xu, S. Gai, F. He, N. Niu, P. Gao, Y. Chen, P. Yang, *J. Mater. Chem. A* **2014**, *2*, 1022.
[4] M. J. Boyd, A. A. Latimer, C. F. Dickens, A. C. Nielander, C. Hahn, J. K. Nørskov, D. C. Higgins, T. F. Jaramillo, *ACS Catal.* **2019**, *9*, 7578.
[5] Y. Y. Birdja, E. Pérez-Gallent, M. C. Figueiredo, A. J. Göttle, F. Calle-Vallejo, M. T. M. Koper, *Nat. Energy* **2019**, *4*, 732.
[6] T. L. Skafte, Z. Guan, M. L. Machala, C. B. Gopal, M. Monti, L. Martinez, E. Stamate, S. Sanna, J. A. Garrido Torres, E. J. Crumlin, M. García-Melchor, M. Bajdich, W. C. Chueh, C. Graves, *Nat. Energy* **2019**, *4*, 846.
[7] L. Wang, F. Song, G. Ozouf, D. Geiger, T. Morawietz, M. Handl, P. Gazdzicki, C. Beauger, U. Kaiser, R. Hiesgen, A. S. Gago, K. Andreas Friedrich, *J. Mater. Chem. A* **2017**, *5*, 3172.
[8] M. S. Burke, L. J. Enman, A. S. Batchellor, S. Zou, S. W. Boettcher, *Chem. Mater.* **2015**, *27*, 7549.
[9] M. Gong, H. Dai, *Nano Res.* **2015**, *8*, 23.
[10] F. Song, L. Bai, A. Moysiadou, S. Lee, C. Hu, L. Liardet, X. Hu, *J. Am. Chem. Soc.* **2018**, *140*, 7748.
[11] H. Jin, J. Wang, D. Su, Z. Wei, Z. Pang, Y. Wang, *J. Am. Chem. Soc.* **2015**, *137*, 2688.
[12] Y. Xu, M. Kraft, R. Xu, *Chem. Soc. Rev.* **2016**, *45*, 3039.
[13] Y. Lin, K.-H. Wu, Q. Lu, Q. Gu, L. Zhang, B. Zhang, D. Su, M. Plodinec, R. Schlögl, S. Heumann, *J. Am. Chem. Soc.* **2018**, *140*, 14717.
[14] Y. Lin, Q. Lu, F. Song, L. Yu, A. K. Mechler, R. Schlögl, S. Heumann, *Angew. Chem. Int. Ed.* **2019**, *58*, 8917.
[15] Y. Ding, M. Greiner, R. Schloegl, S. Heumann, *ChemSusChem* **2020**, *13*, 4064.
[16] X. Lu, W.-L. Yim, B. H. R. Suryanto, C. Zhao, *J. Am. Chem. Soc.* **2015**, *137*, 2901.
[17] K. Shinozaki, J. W. Zack, S. Pylypenko, R. M. Richards, B. S. Pivovar, S. S. Kocha, *Int. J. Hydrogen Energy* **2015**, *40*, 16820.
[18] S. Bhandari, P. V. Narangoda, S. O. Mogensen, M. F. Tesch, A. K. Mechler, *ChemElectroChem* **2022**, *9*.
[19] H.-S. Oh, H. N. Nong, T. Reier, A. Bergmann, M. Gliech, J. Ferreira de Araújo, E. Willinger, R. Schlögl, D. Teschner, P. Strasser, *J. Am. Chem. Soc.* **2016**, *138*, 12552.
[20] B. Li, X. Sun, D. Su, *Phys. Chem. Chem. Phys.* **2015**, *17*, 6691.
[21] Z. Lin, G. H. Waller, Y. Liu, M. Liu, C.-P. Wong, *Carbon* **2013**, *53*, 130.
[22] Z. Luo, S. Lim, Z. Tian, J. Shang, L. Lai, B. MacDonald, C. Fu, Z. Shen, T. Yu, J. Lin, *J. Mater. Chem. A* **2011**, *21*, 8038.
[23] Y. Lin, Y. Zhu, B. Zhang, Y. Ahm Kim, M. Endo, D. Su, *J. Mater. Chem. A* **2015**, *3*, 21805.
[24] Z. Zhao, M. Li, L. Zhang, L. Dai, Z. Xia, *Adv. Mater.* **2015**, *27*, 6834.
[25] D. Guo, R. Shibuya, C. Akiba, S. Saji, T. Kondo, J. Nakamura, *Science* **2016**, *351*, 361.
[26] Y. Yi, G. Weinberg, M. Prenzel, M. Greiner, S. Heumann, S. Becker, R. Schlögl, *Catal. Today* **2017**, *295*, 32.
[27] S. Möller, S. Barwe, J. Masa, D. Wintrich, S. Seisel, H. Baltruschat, W. Schuhmann, *Angew. Chem. Int. Ed.* **2020**, *59*, 1585.
[28] Y. Yi, J. Tornow, E. Willinger, M. G. Willinger, C. Ranjan, R. Schlögl, *ChemElectroChem* **2015**, *2*, 1929.
[29] Y. Li, J. Li, Y.-G. Wang, X. Chen, M. Liu, Z. Zheng, X. Peng, *Int. J. Hydrogen Energy* **2021**, *46*, 13273.
[30] Y. Lin, Z. Liu, L. Yu, G.-R. Zhang, H. Tan, K.-H. Wu, F. Song, A. K. Mechler, P. P. M. Schleker, Q. Lu, B. Zhang, S. Heumann, *Angew. Chem. Int. Ed.* **2021**, *60*, 3299.
[31] L. Zhang, F. Zhang, X. Yang, G. Long, Y. Wu, T. Zhang, K. Leng, Y. Huang, Y. Ma, A. Yu, Y. Chen, *Sci. Rep.* **2013**, *3*, 1408.

[32] Y. Lin, D. Su, *ACS Nano* **2014**, *8*, 7823.
[33] B. Avasarala, R. Moore, P. Haldar, *Electrochim. Acta* **2010**, *55*, 4765.
[34] R. Arrigo, M. Haevecker, S. Wrabetz, R. Blume, M. Lerch, J. McGregor, E. P. J. Parrott, J. A. Zeitler, L. F. Gladden, A. Knop-Gericke, R. Schloegl, D. S. Su, *J. Am. Chem. Soc.* **2010**, *132*, 9616.
[35] R. J. J. Jansen, H. van Bekkum, *Carbon* **1995**, *33*, 1021.
[36] L. Zhao, L.-Z. Fan, M.-Q. Zhou, H. Guan, S. Qiao, M. Antonietti, M.-M. Titirici, *Adv. Mater.* **2010**, *22*, 5202.
[37] P. N. Ross, H. Sokol, *J. Electrochem. Soc.* **1984**, *131*, 1742.
[38] K. Y. Shi, S. D. Yin, X. X. Tao, Y. Du, H. He, Z. P. Lv, N. Xu, *Energy Sources Part A* **2013**, *35*, 1456.
[39] D. M. Kolb, M. Przasnyski, H. Gerischer, *J. Electroanal. Chem.* **1974**, *54*, 25.
[40] W. Hansen, G. Hansen, *Surf. Sci.* **2001**, *481*, 172.
[41] C. Mo, J. Jian, J. Li, Z. Fang, Z. Zhao, Z. Yuan, M. Yang, Y. Zhang, L. Dai, D. Yu, *Energy Environ. Sci.* **2018**, *11*, 3334.
[42] P. H. Matter, L. Zhang, U. S. Ozkan, *J. Catal.* **2006**, *239*, 83.
[43] I. Duo, C. Levy-Clement, A. Fujishima, C. Comninellis, *J. Appl. Electrochem.* **2004**, *34*, 935.
[44] J. W. Straten, P. Schleker, M. Krasowska, E. Veroutis, J. Granwehr, A. A. Auer, W. Hetaba, S. Becker, R. Schlögl, S. Heumann, *Chem. Eur. J.* **2018**, *24*, 12298.
[45] A. A. Ramadan, R. D. Gould, A. Ashour, *Thin Solid Films* **1994**, *239*, 272.

Manuscript received: October 28, 2022
Revised manuscript received: January 20, 2023

RESEARCH ARTICLE

Curbing corrosion: Nitrogen functionalized carbon-based electrode materials have been synthesized and analysed in comparison to pure carbon-based electrodes. Analysis of the gaseous products shows a higher proportion of electrocatalytic water splitting due to the higher oxygen gas product for N-containing electrodes, consequently less carbon corrosion.

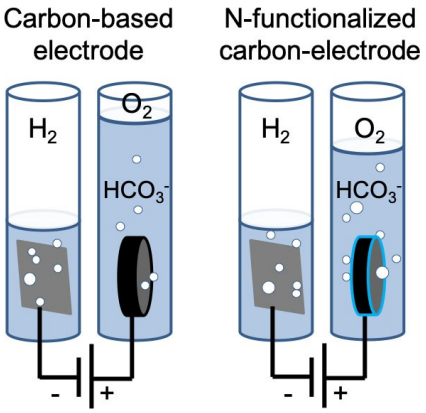

Dr. F. Song, Dr. J. W. Straten, Dr. Y.-M. Lin, Dr. Y. Ding, Prof. Dr. R. Schlögl, Dr. S. Heumann, Prof. Dr. A. K. Mechler**